Joint Special Interest Group meeting between euspen and ASPE
Advancing Precision in Additive Manufacturing
Inspire AG, St. Gallen, Switzerland 2021
www.euspen.eu

Testing the similarity conditions in the CT measurement of additively manufactured lattice structures

M. Praniewicz[1], M. Ferrucci[1], J. Fox[1], C. Saldana[2]

1National Institute of Standards and Technology, USA*
[2]Georgia Institute of Technology, USA

maxwell.praniewicz@nist.gov

Abstract
X-ray computed tomography (CT) enables the non-destructive measurement of hidden internal features that are inaccessible by tactile or optical coordinate measuring systems. This makes CT the technology of choice for inspecting complex components made by additive manufacturing (AM), lattice structures being a prime example. Uncertainty assessment in CT dimensional measurements is limited to the substitution method, which prescribes strict similarity conditions between the test object and a separate, calibrated reference object. The notoriously rough surfaces and form deviations in AM components present a challenge in terms of ensuring similarity with respect to the idealized reference object, particularly as these deviations pertain to changes in X-ray penetration lengths during CT measurement. Currently, though, there is no literature on how to quantify 'similarity' and to what extent these conditions can be stressed while ensuring that uncertainty in the CT measurement of AM parts can be correctly determined. In this study, we investigate the effect that varying degrees of dissimilarity in object shape and size have on the image quality of their tomographic reconstruction in the context of establishing a quantitative measure of similarity.

X-ray computed tomography, Lattice structures, Similarity

1. Introduction

Lattice structures produced using additive manufacturing (AM) can provide improved stiffness/weight, energy absorption, heat transfer, and bio-integration of conventionally designed components [1–3]. X-ray computed tomography (XCT) is widely used to non-destructively characterize lattice structures, e.g., for mechanical testing [4–7]. However, XCT measurements succumb to various uncertainty contributors, including the material and geometric characteristics of the object to be measured. Uncertainty in the XCT measurement of lattices has been studied to a limited extent [8, 9]. In general, the assessment of uncertainty in CT is limited to the substitution method, which is described in the VDI/VDE 2630-2.1 guideline [10]. This approach relies on the presence of a separate, calibrated reference object that meets strict similarity conditions in terms of material, shape, and size with respect to the test object. The similarity conditions are specified to ensure that bias, repeatability, and other uncertainty components determined from the measurement of the reference object are equally applicable to the measurement of the test object. In other words, the response of the CT system to any differences between reference and test objects should be approximately linear [11].

The notoriously rough surfaces of AM components present a challenge in terms of ensuring similarity, particularly in terms of shape and size, between as-built test objects and the corresponding reference objects, which are typically manufactured with smooth surfaces to enable low uncertainty calibration of the relevant measurands by tactile coordinate measuring machine (CMM). These geometric dissimilarities can result in significant differences in X-ray penetration length during the CT measurement of small, complex parts such as lattice structures.

The non-linear relationship between penetration length and polychromatic X-ray absorption, i.e., the term in the exponent of the Beer-Lambert equation, and the monochromaticity assumed in conventional tomographic reconstruction algorithms result in so-called beam hardening artifacts. Differences in penetration lengths between reference and test object will result in different manifestations of beam hardening artifacts in the reconstructed volumes, which can compromise the similarity conditions prescribed in VDI/VDE 2630-2.1 guidelines. However, there is currently no literature on how to quantify 'similarity' and to what extent these conditions can be stressed while ensuring that uncertainty in the CT measurement of AM parts can be correctly determined. In this study, we investigate the effect that varying degrees of dissimilarity in object shape and size have on the image quality of their tomographic reconstruction in the context of establishing a quantitative measure of similarity.

To simulate the effect of AM-induced form errors, several test lattice objects are designed with varying strut diameters. Polychromatic cone beam CT acquisitions of the test objects are simulated, and each dataset is subsequently reconstructed using conventional Feldkamp-Davis-Kress (FDK) filtered back projection. The similarity between the various reconstructed test objects is determined using a slightly modified

* Certain commercial entities, equipment, or materials may be identified in this document to describe an experimental procedure or concept adequately. Such identification is not intended to imply recommendation or endorsement by the National Institute of Standards and Technology, nor is it intended to imply that the entities, materials, or equipment are necessarily the best available for the purpose.

implementation of the contrast discrimination function (CDF) described in ASTM E1695 [12]. The same image quality metric is then applied to the simulated measurement of a realistic test lattice (defined by the surface model extracted from a previous experimental CT measurement).

2. Methodology

A lattice-like structure with structs of 0.5 mm nominal diameter (Figure 1a) was additively manufactured with the struts oriented horizontally with respect to the build direction. This AM component was then scanned using XCT and processed in VGStudio MAX 3.4 (Figure 1 b) [13]. Cylinders were then least-squares fit to each strut and the cylindricity error was evaluated. Figure 1c displays the cylindrical form error of one strut. Across the nine cylinders of the structure, form errors of approximately ±0.15 mm were observed. The magnitude of these form errors was used to guide the experiment conducted in this work.

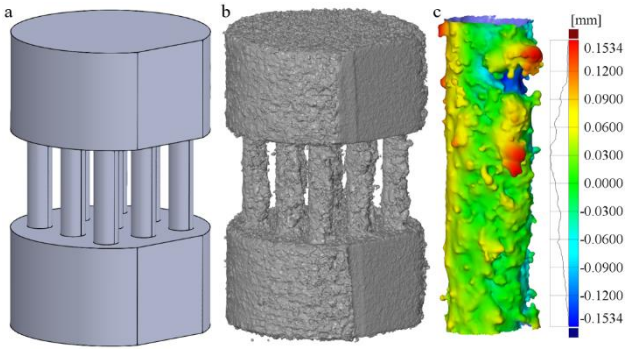

Figure 1. Example of form error in AM lattice components: (a) Component design geometry with strut diameter 0.5 mm, (b) Surface model of manufactured AM component acquired though XCT, (c) Example cylindricity error in a single AM strut

2.1. XCT Simulation

Monochromatic and polychromatic XCT acquisitions were simulated using aRTist software [14]. Five cylinder arrays similar to the lattice-like structure in Figure 1 were simulated, each array comprising different cylinder diameters (0.3 mm, 0.4 mm, 0.5 mm, 0.6 mm, 0.7 mm). The acquisition geometry (a), the polychromatic X-ray spectrum (b), an example projection (c), and a sample slice of the reconstructed volume (d) can be seen in Figure 2. The simulation parameters are shown in Table 1. The polychromatic X-ray spectrum was generated using source parameters from an actual industrial X-ray source at the Georgia Institute of Technology, while the energy in the monochromatic simulations was given by the weighted mean the polychromatic spectrum, similar to the average energy in [15]. Noise and unsharpness (geometric or detector) were not included in the simulated acquisitions.

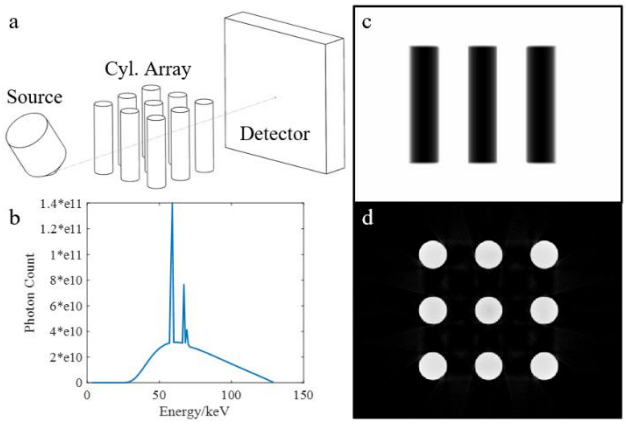

Figure 2. XCT Simulation: (a) Simulation configuration (not to scale), (b) Source spectrum used in polychromatic simulations, (c) Sample polychromatic project (0.5 mm diameter), (d) Sample central slice from polychromatic reconstruction (0.5 mm diameter)

Table 1 XCT Simulation Parameters

Parameter		Value
Source	Target material	W
	Target angle	45°
	Window material	Be
	Window thickness	0.2 mm
	Acceleration voltage	130 kV
	Current	0.061 mA
	Physical filter	0.5 mm Cu
	Energy (mono)	71.2 keV
Detector	Pixel size	0.127 mm
	Number of pixels (WxH)	500 x 350
	Source to detector distance	803.359 mm
Object Positioning	Source to rotation axis distance	60.506 mm
Data acquisition	Number of projections	900
	Reconstruction algorithm	FDK
	Bit depth (reconstruction)	32bit

2.2. XCT Data analysis

The reconstructed volumes were imported into MATLAB and processed using a modified implementation of the technique to determine the CDF described in ASTM E1695 [12]. For each volume, background correction was first performed by subtracting from all voxel-wise gray values in the volume the average voxel value in the background, defined as the region from the blue box to the lateral edges of the volume defined in Figure 3a. A global threshold value was calculated utilized using the ISO50 method for the entire volume and was used to determine the boundary between the material and background for the volume. The central slice along the rotational axis of the volume was then isolated for analysis in this study.

Regions of interest were created around each cylinder in the central slice (shown as red squares in Figure 3) to enable cylinder-wise analyses. The CDF was calculated for each region using the tiling method described in ASTM E1695. It is recommended that the tile size (D^*) is increased until *"…the size*

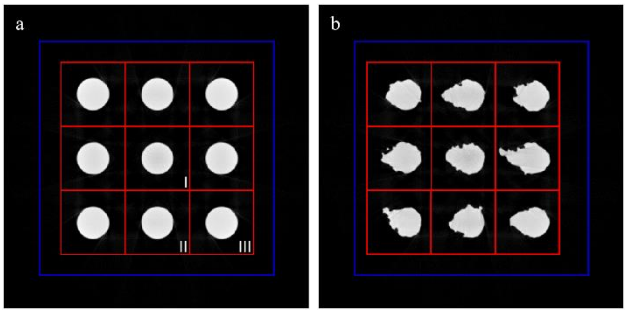

Figure 3. Central slices through reconstructed cylinder arrays. (a) Middle reconstruction slice (0.5 mm diameter). The region outside the blue square and to the outer edges of the slice was used for background compensation. The regions inside the red boxes indicate the regions of interest for each cylinder. (b) Middle reconstruction slice of AM lattice model (0.5 mm nominal diameter).

of the tiles becomes too large to obtain a statistically significant number of tiles. It is recommended that the minimum number of tiles is about 25" [12]. While this recommendation is reasonable for the XCT measurement of the relatively larger cylindrical phantom prescribed in ASTM E1695, it is generally difficult to satisfy when measuring the small struts of lattice structures. Hence, in this work, the minimum number of tiles for a given D^* is set to 4. The results of the reconstructions were assumed to be axisymmetric with respect to the lateral axes of the volumes, and therefore only the results of the center cylinder (I in Figure 3), a side cylinder (II in Figure 3), and a corner cylinder (III in Figure 3) were evaluated. Monochromatic and polychromatic acquisitions of the AM component surface model shown in Figure 1b were also simulated. The CDFs of these simulations were determined using the previously described method.

3. Results

Ideal cylinder arrays

The center cylinder of the array is subject to stronger cupping artifacts than the other cylinders. Figure 4 displays the CDF curves of the center cylinder for both monochromatic and polychromatic simulations in the 0.3 mm, 0.5 mm, and 0.7 mm diameter cylinder arrays. All monochromatic scans appear to show an approximately linear decrease in the CDF value with increasing D^*. This indicates that only statistical noise is observed in the monochromatic scans, as pure statistical noise should follow a slope of -1 on the log-log plot [12]. This observation was made in the monochromatic simulations of all cylinder diameters. In the polychromatic simulations, the CDF of the 0.3 mm diameter cylinder closely follows its monochromatic CDF but deviates at larger values of D^*. As D^* increases, the number of tiles used in the CDF calculation continues to drop until the predefined minimum of 4. With a low sample size, a higher variance in the CDF values is expected. However, the polychromatic CDFs of the 0.5 mm and 0.7 mm diameter cylinders depart from their monochromatic CDFs at low values of D^*, indicating an increased variation in reconstructed gray values within the cross section of the cylinder, i.e., more pronounced cupping artifacts. This departure increases with increasing cylinder diameter.

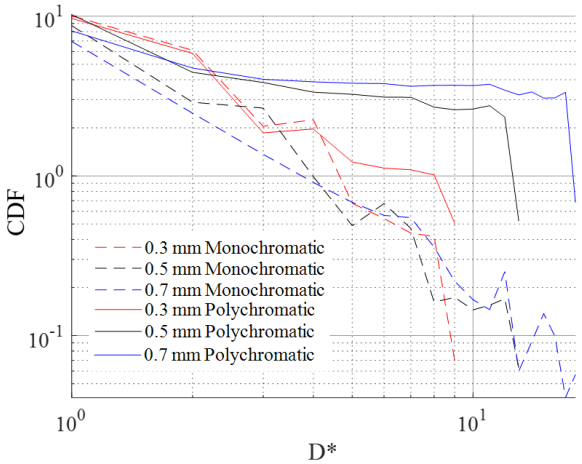

Figure 4. CDF curves for the center cylinder of both monochromatic and polychromatic simulations in 0.3 mm, 0.5 mm, 0.7 mm diameter arrays

To further examine this behavior, the CDF acquired from the monochromatic simulations (CDF_M) was subtracted from the CDF acquired from the polychromatic simulations (CDF_P) for all arrays. Figure 5 displays these results for the center cylinder at all diameters; as the diameter of the cylinder array increases, CDF_P increasingly deviates from CDF_M. This trend is expected as there are stronger cupping artifacts in larger cylinders.

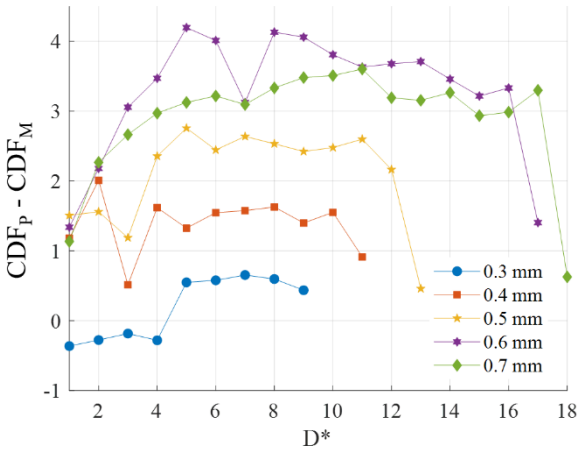

Figure 5. Difference between CDF_P and CDF_M in the center cylinder for all diameters

Figures 6 and 7 show the difference between CDF_P and CDF_M for the side and corner cylinders, respectively, of each array. A reduction in magnitude between the side and corner cylinders, and the center cylinder is apparent. This behavior is expected, as the side and corner cylinders are subject to reduced cupping artifacts. The average difference in CDF value is observed to be lower in the corner cylinders for the 0.3 mm, 0. 4 mm, and 0.5 mm compared to the side cylinders. Interestingly, this trend is not observed in the 0.6 mm and 0.7 mm diameter arrays.

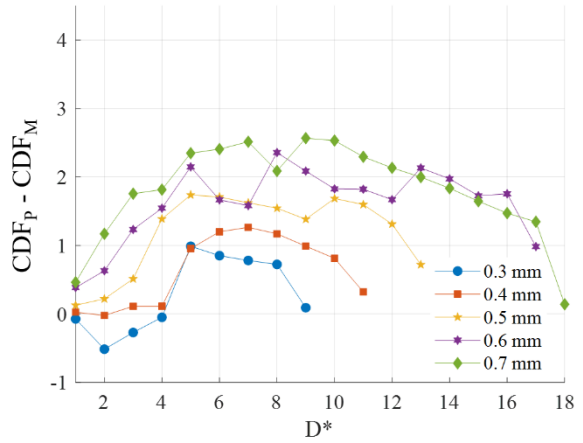

Figure 6. Difference between CDF_P and CDF_M in the side cylinder for all diameters

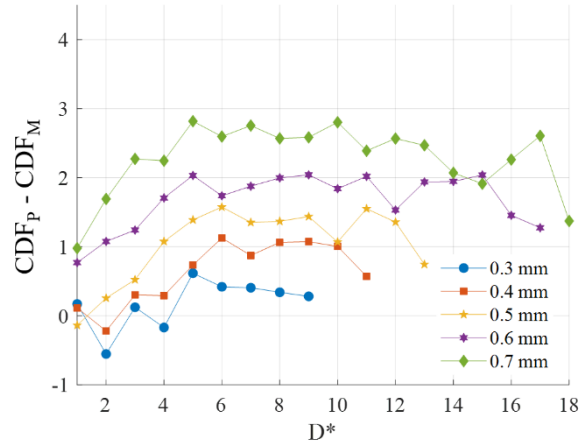

Figure 7. Difference between CDF_P and CDF_M in the corner cylinder for all diameters

AM cylinder array

Figure 8 displays the difference between CDF_P and CDF_M for three cylinders (center, side, and corner) in the AM component. Differences in the plot trends between the ideal cylinder arrays

and the AM component are immediately noted. A much higher difference between the CDF_P and CDF_M is observed at $D^* = 1$ for all three cylinders, indicating a much higher standard deviation of voxel-wise gray values in the polychromatic simulation. Upon closer visual examination of the reconstructed slice, windmill artifacts (due to aliasing in the reconstruction of sharp edges) were noted.

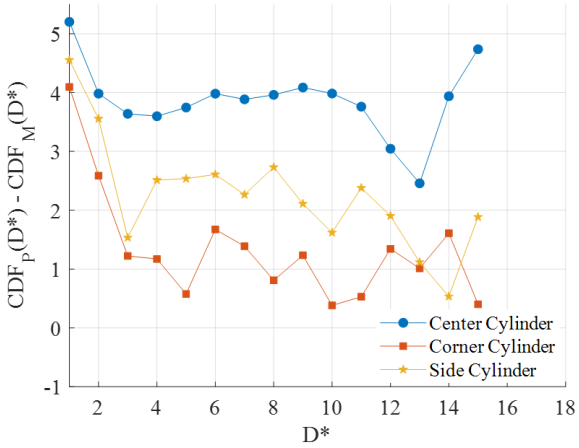

Figure 8. CDF curves for AM component

Nevertheless, the trend observed in Figures 5, 6, and 7, in which the difference between the polychromatic and monochromatic simulations increases as the cylinder in question becomes more central in the array for 0.5 mm diameter, is also observed here. The internal gray values, normalized here with respect to the highest and lowest gray values in the region of interest, on the different cylinder locations are investigated. While the gray values of the monochromatic simulations are relatively uniform across the cross section of the cylinder, with minor fluctuations due to statistical variation, the gray values in the polychromatic simulation are not uniform. Figure 9 displays the normalized gray values for the center, side, and corner cylinders in the 0.7 mm diameter array. Significant variations in the gray values across the cross-sectional area of the cylinder can be observed as a function of cylinder position. This variation could explain why the CDF results between the side and corner cylinders in the 0.6 mm and 0.7 mm diameter arrays did not appear to follow the same trend as in the other diameters. While the CDF appears to detect some differences between the cylinders, it is not able to capture changes in the gray value distribution across the cross-sectional area of the cylinder. It is not entirely clear at what point the presented results are definitively dis-similar. Furthermore, it is not immediately apparent that the results from the various arrays are similar. Thus, this raises a question regarding similarity analysis: in the comparison of two sets of results, should the null hypothesis be similarity or dis-similarity.

It should be noted that the authors also attempted to evaluate the spatial resolution of each dataset using the methodology described in ASTM E1695. However, the described methodology could not be applied to the AM component, as form errors would invalidate the creation of the edge response function.

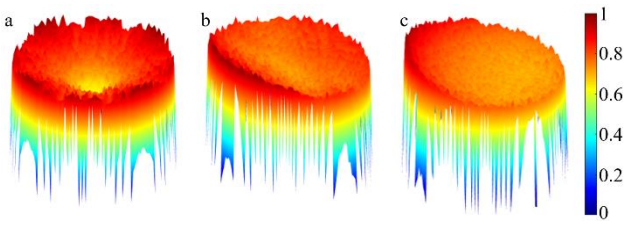

Figure 9. 3D surface plots of the relative internal intensity of various cylinders in the 0.7 mm diameter array: (a) Center cylinder (b) Side cylinder (c) Corner cylinder

4. Conclusion

There is currently no quantitative basis with which we can assert sufficient similarity to warrant the use of the substitution method for a test object deviating, e.g., in terms of X-ray penetration length, from the reference object. In this study, we investigate the use of the CDF, an image quality metric prescribed in ASTM E1695, to expose differences in the manifestation of cupping artifacts due to differences in X-ray penetration lengths. These results indicate that changes in form error can potentially lead to significant variations in CDF within a lattice structure. Furthermore, these results show that variations in the CDF can also occur between individual struts of a lattice based on their position. Future work will investigate new approaches to determine spatial resolution that are robust to non-ideal geometries, and will evaluate the efficacy of other metrics as measures of similarity. This and future studies should stimulate discussions and further work on determining a cut-off for similarity based on these metrics.

References

[1] A. Nazir *et al.*, "A state-of-the-art review on types, design, optimization, and additive manufacturing of cellular structures," *Int. J. Adv. Manuf. Technol.*, vol. 104, no. 9, pp. 3489–3510, Oct. 2019, doi: 10.1007/s00170-019-04085-3.

[2] B. K. Nagesha *et al.*, "Review on characterization and impacts of the lattice structure in additive manufacturing," *Mater. Today Proc.*, vol. 21, pp. 916–919, Jan. 2020, doi: 10.1016/j.matpr.2019.08.158.

[3] A. du Plessis *et al.*, "Beautiful and Functional: A Review of Biomimetic Design in Additive Manufacturing," *Addit. Manuf.*, vol. 27, pp. 408–427, May 2019, doi: 10.1016/j.addma.2019.03.033.

[4] A. D. Dressler *et al.*, "Heterogeneities Dominate Mechanical Performance of Additively Manufactured Metal Lattice Struts," *Addit. Manuf.*, 2019, doi: https://doi.org/10.1016/j.addma.2019.06.011.

[5] M. Dallago *et al.*, "On the effect of geometrical imperfections and defects on the fatigue strength of cellular lattice structures additively manufactured via Selective Laser Melting," *Int. J. Fatigue*, vol. 124, pp. 348–360, 2019, doi: https://doi.org/10.1016/j.ijfatigue.2019.03.019.

[6] C. Yan *et al.*, "Evaluations of cellular lattice structures manufactured using selective laser melting," *Int. J. Mach. Tools Manuf.*, vol. 62, pp. 32–38, 2012, doi: https://doi.org/10.1016/j.ijmachtools.2012.06.002.

[7] D. Ashouri *et al.*, "Mechanical behaviour of additive manufactured 316L f2ccz lattice structure under static and cyclic loading," *Int. J. Fatigue*, vol. 134, p. 105503, 2020, doi: https://doi.org/10.1016/j.ijfatigue.2020.105503.

[8] F. Zanini *et al.*, "Uncertainty of CT dimensional measurements performed on metal additively manufactured lattice structures," presented at the 10th Conference on Industrial Computed Tomography, 2020.

[9] M. Praniewicz *et al.*, "An exploration of XCT measurement of AM lattice structures: Uncertainty in calibrated reference object measurement. (Under review)," *Precis. Eng.-J. Int. Soc. Precis. Eng. Nanotechnol.*, 2021.

[10] Verein Deutscher Ingenieure (VDI), "VDI/VDE 2630 Blatt 2.1 Computed tomography in dimensional measurement: Determination of the uncertainty of measurement and the test process suitability of coordinate measurement systems with CT sensors," Düsseldorf, Germany, 2015.

[11] M. Ferrucci *et al.*, "Charting the course towards dimensional measurement traceability by X-ray computed tomography," *Meas. Sci. Technol.*, Mar. 2021, doi: 10.1088/1361-6501/abf058.

[12] ASTM International, "ASTM E1695 - 20: Standard Test Method for Measurement of Computed Tomography (CT) System Performance," ASTM International, West Conshohocken, PA, 2020.

[13] Volume Graphics GmbH, "VGStudioMax 3.4".

[14] C. Bellon *et al.*, "Radiographic simulator aRTist: version 2," 2012.

[15] A. M. Hernandez *et al.*, "Tungsten anode spectral model using interpolating cubic splines: Unfiltered x-ray spectra from 20 kV to 640 kV," *Med. Phys.*, vol. 41, no. 4, Art. no. 4, 2014.